

# CFD modeling of the in-cylinder flow in a variable-compression spark-ignited engine

A. HATZIAPOSTOLOU, G. RAPTIS  
 Energy Technology Department  
 Technological Educational Institute of Athens  
 Ag. Spyridonos str., 12210, Athens  
 GREECE  
<http://www.et.teiath.gr>

*Abstract:* - Three dimensional flow calculations of the operation cycle of a small 4-stroke variable compression spark-ignited engine have been performed for different engine speeds under full load conditions. The compression ratio at the laboratory engine is adjusted within the range of 4 to 10, by means of a special piston, which moves manually and alters accordingly the combustion chamber volume. Calculations were performed for three different engine speeds and two compression ratios. Ensemble-averaged velocity data are presented in two main forms: velocity magnitude at characteristic points as a function of crank angle and two-dimensional vector plots at characteristic cross sections inside the combustion chamber at specific crank angles. The results confirm that the in-cylinder flow field scales well with the engine speed and that increasing the compression ratio results in more pronounced large scale flow-field effects, such as the tumbling motion generated during the induction stroke and persisting through the compression stroke.

*Key-Words:* Computational Fluid Dynamics modeling, internal combustion engine, variable compression ratio, in-cylinder flow

## 1 Introduction

During the last few decades, internal combustion engines have been greatly improved in terms of efficiency and reduction of pollutant emissions [1, 4]. This trend must continue in the near future, since international organizations and governments are issuing more severe emissions restrictions for passenger cars. At the same time, although new concepts have appeared as alternatives to the IC engine, such as fuel cells [6], it seems that it will take several decades for them to mature enough for large scale production. It follows that the internal combustion engine will remain as the major power source for automobiles, even if it will be part of a hybrid package, either Otto-electric or Diesel-electric.

In spark-ignition engines, the majority of commercial engines still use port-fuel injection to generate a homogeneous-charge in the cylinder. During the last few years, stratified-charge direct-injection gasoline engines have appeared in commercial form, following in-depth investigations for the last two decades, combining experimental and theoretical calculations. The latter were made possible through the use of reliable commercial computational fluid dynamics (CFD) codes, which have been developed and validated extensively.

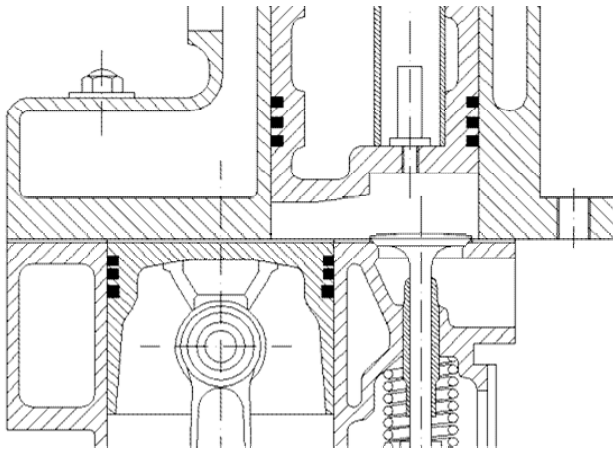
CFD codes are and will remain a valuable tool in the design of improved engines of all kinds

The present study investigates the in-cylinder flowfield and combustion of a small laboratory homogeneous-charge variable-compression single-cylinder spark-ignited engine. The main motivation is to study the combined effect of engine speed and compression ratio on the flowfield during the induction and compression strokes, as well as the combustion process.

## 2 Case Description

The engine studied in this paper is a Petter W1 model modified by Plint, in order to be able to adjust the compression ratio. A cross-section of the engine combustion chamber, as well as its main characteristics, are presented in Fig.1. The engine is equipped with one intake and one exhaust side valve, with the camshaft situated close to the crankshaft. This is quite an old design, which presents a big advantage in the present case: it is quite easy to incorporate a manually-adjusted piston in the engine head, which, by moving up or down, alters the engine volume at top-dead-center (TDC). At the top right corner of Fig 1, the bottom half of this piston can be seen, as well as the spark plug situated just opposite of the valves. A better

representation of the engine configuration can be seen in Fig. 2, where the cross-section is presented in 3-D. It becomes evident that the shape of the combustion chamber with the inserts for the two valves, as well as the passage to the main cylinder is quite complex, compared with a conventional 2 or 4-valve spark-ignited engine. The latter required considerable effort in developing the grid for the CFD calculations, dictating the division of the chamber volume in several zones with different grid characteristics.



Bore	85mm
Stroke	82.5mm
Swept volume	468cc
Compression ratio	4:1 to 10:1
Maximum speed	2500 rpm

Fig. 1 Cross-section of the modified Peter W1 engine combustion chamber and its main geometrical characteristics.

### 3 Numerical Methodology

A finite volume commercial CFD code was employed in order to solve the discretised Navier-Stokes equations [2]. The standard  $k-\epsilon$  turbulence model for high Reynolds numbers with standard wall functions is used for model closure. The code is based on the pressure-correction method [5], using the PISO algorithm. The first order upwind differencing scheme is used in the discretisation of momentum and turbulence equations.

The temporal discretisation is implicit on the variable time step depending on the stage of the 4-stroke cycle. When the valve lift is small, at the beginning and at the end of the intake stroke, velocities at the valve jet are expected to be high. It follows that the time step must be in the range of  $0.1^\circ$  crank angle (CA), in order to comply with the convergence criterion. During the middle phase of

the intake stroke and most of the compression stroke, the time step was doubled to save processing time and was reduced again towards the end of the compression stroke and, especially, during the combustion phase. The latter was simulated using the turbulent premixed combustion model of Zimont, which involves the solution of a transport equation for the reaction progress variable [7, 9]. The closure of this equation is based on the definition of the turbulent flame speed, which is computed using a model for wrinkled and thickened flame fronts [8]. The main assumption in the Zimont model is that it considers the reacting flow field to be divided into regions of burnt and unburnt species, separated by a moving thin flame sheet.

For each case, the calculation begins at the inlet valve opening which is  $6^\circ$  CA before the TDC of induction and ends at  $240^\circ$  CA after the TDC of combustion. The initial turbulence intensity level was set at 10% of the mean flow, which is large enough for the flow to be considered fully turbulent. Constant pressure boundary conditions were assigned at both inlet and outlet valves and all walls were considered adiabatic.

### 4 Grid independence study

The computational domain includes both intake and outlet ports and valves, the combustion chamber and the cylinder. The grid developed can be seen in Fig. 3.

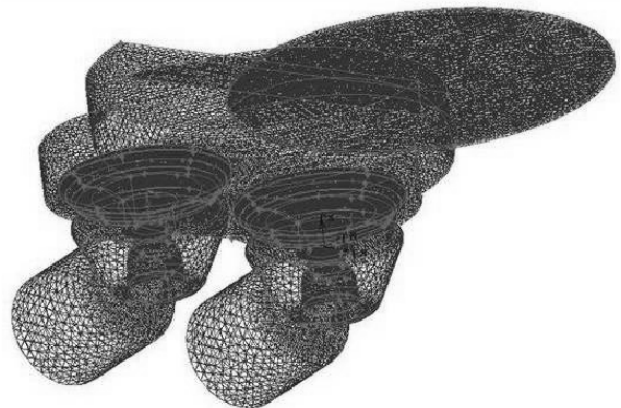


Fig. 3. Computational grid at TDC together with inlet and outlet ports

The number of cells varies between 245000 at TDC to 376000 at bottom-dead-center (BDC). The majority of the cells used were hexahedral, since they provide better accuracy and stability than tetrahedral. The combustion chamber was divided in six zones; each zone has been meshed separately. This technique is very useful to obtain a good quality grid and to reduce the time of the meshing

procedure. The connectivity of the various zones is achieved by means of arbitrary interfaces that connect common faces of adjacent sub-domains. Tetrahedral cells have been used in the areas where the “moving and deforming mesh” concept was employed. During the compression stroke once the intake valve is closed, the intake port sub-domain is disconnected from the calculation, so that to save CPU time; the same applies to the outlet port.

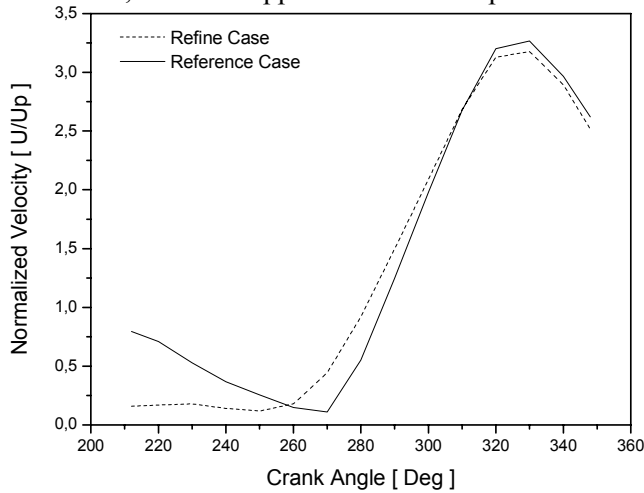


Fig. 4. Velocity magnitude comparison for grid independence study

In order to ensure grid independence and improved accuracy of the results, two calculations during the compression stroke were performed using two different grids: the reference grid was the one already presented and the second was refined in certain areas where steep gradients are expected. Fig 4 depicts the velocity magnitude during the compression stroke at a point near the inlet valve. It can be easily deduced that there are no significant differences between the two cases, therefore all subsequent calculations were performed with the reference grid.

### 5 Results and discussion

Five cases were examined and analyzed: at the low compression ratio of 5.7, the engine speed settings at full load were 750 rpm, 1200 rpm and 2000 rpm, whereas at the high compression ratio of 10, the engine speed settings at full load were 1200 rpm and 2000 rpm. It is worth noting that these speed settings cover almost the whole operating range of the laboratory engine; the maximum speed of 2500 rpm was not examined, because it was considered unsafe to operate the specific engine at this level. The present investigation is accompanied by parallel experimental measurements for comparison

purposes, which will be included in a future publication

Ensemble-averaged mean velocity data are presented in two main forms: velocity magnitude at characteristic points as a function of crank angle and two-dimensional vector plots at characteristic cross sections inside the cylinder and combustion chamber at specific crank angles. All velocity data are in dimensionless form, as they are normalized by the mean piston speed (denoted hereafter as  $V_p$ ), which is 2.0625 m/s, 3.3 m/s and 5.5 m/s at 750 rpm, 1200 rpm and 2000 rpm, respectively. Fig. 5 depicts the locations of the points within the combustion chamber, which were selected for presentation: point A is within the spark gap, point B is close to the inlet valve and point C is at the top center of the main engine cylinder.

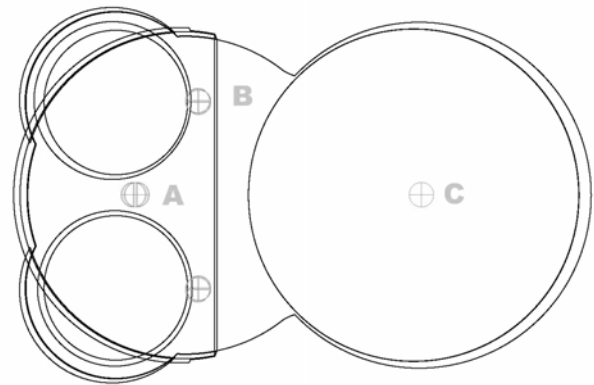


Fig. 5. Locations of the points under investigation within the cylinder and chamber volume (top view)

Fig. 6 presents the mean velocity magnitude at point A as a function of CA during most of the operating cycle.

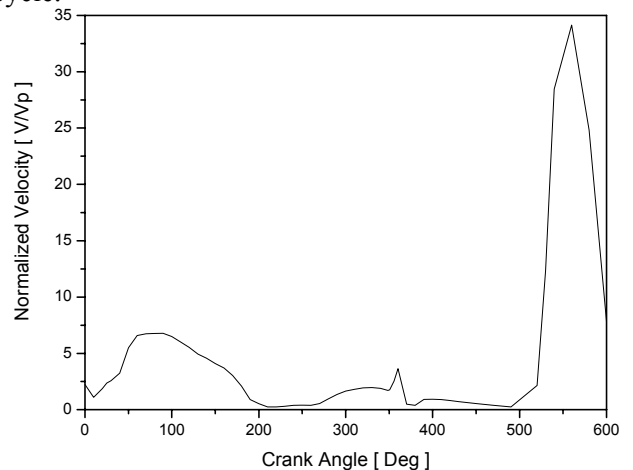


Fig. 6. Mean velocity magnitude at point A vs. CA, 1200rpm, CR=5.7

The engine speed in this case is 1200 rpm and the compression ratio is 5.7. The zero value of CA corresponds to the TDC of induction and the value

360° corresponds to the TDC of compression. The same applies to all CA values in the subsequent graphs. During the induction stroke, the maximum mean velocity magnitude presents a maximum of almost 7Vp (seven times the mean piston speed) at around 83° CA after the TDC of induction. This can be attributed to the close proximity of point A to the inlet valve. Later on during the induction stroke, the velocity magnitude drops at 2Vp at BDC and 0.4Vp at the inlet valve closure, which is at 25° CA after BDC. During the compression stroke the velocities remain low, as the piston movement does not affect the spark area, due to the rather unconventional design of the specific engine configuration. There is a local maximum of 3.6Vp at the TDC of compression, which is directly related to the onset of combustion. The velocities remain low during the expansion stroke and start to increase abruptly after the BDC with a maximum value of 34Vp at 20° CA after the BDC of expansion. The latter is attributed to the exhaust valve, which opens at 25° CA before the BDC of expansion (EVO - exhaust valve opening).

In order to study in detail the effect of engine speed during the induction and compression stroke, all three engine speeds examined that correspond at the same point A are presented in Fig. 7.

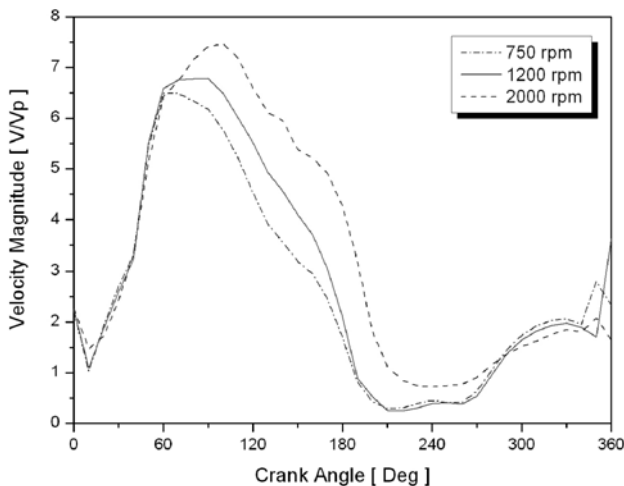


Fig. 7. Mean velocity variations at point A vs. CA at three eng. speeds, CR=5.7

The general trend is that the normalized velocity patterns are quite similar, confirming the fact that the in-cylinder flow-field scales well with engine speed. This is particularly true until 60° CA after the TDC of induction. However, later on, there is a clear deviation from that rule: increasing the engine speed, results in higher normalized velocity magnitude at a later stage during induction (compare graphs at 70 - 180° CA). This is probably related to higher momentum effects due to the increasing engine speed.

Fig. 8 includes velocity magnitude data for the two compression ratios studied (low, CR=5.7 and high, CR=10) at the same point A and at the engine speeds of 1200 and 2000 rpm.

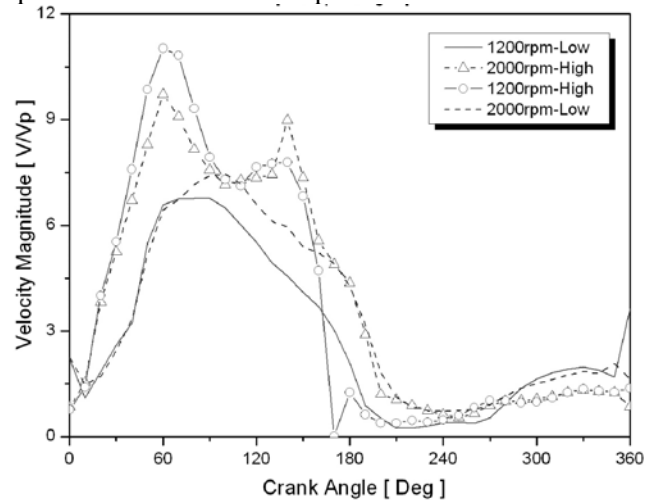


Fig. 8. Mean velocity variations at point A vs. CA at two eng. speeds, and two CR=5.7, low and CR=10, high

It becomes evident that the increase of the compression ratio significantly modifies the velocities from very early at the induction stroke. At 1200 rpm, the maximum value of the normalized velocity magnitude during induction increases by approximately 75%, (from 6.8Vp to 11Vp), when the compression ratio increases by 62% (from 5.7 to 10). In qualitative terms, the same applies at the higher engine speed of 2000 rpm. The velocity magnitude evolution during induction is also affected, especially in the case of 2000rpm, with a second local maximum appearing at 145°CA. It follows that the compression ratio has a more pronounced effect than speed on the in-cylinder flow-field and this can be attributed to the fact that the in-cylinder flow is a mainly a pressure-driven phenomenon. It is also worth noting that, after the IVC (inlet valve closure at 25° CA after BDC) and during the compression stroke, all four velocity patterns appear similar, confirming that the flow scaling with engine speed is the dominant factor during the compression stroke

Fig. 9 presents velocity magnitude data at point B, which is close to the inlet valve. The engine speed effect at this point is less apparent as evidenced by the similarity of all three graphs covering the engine speed operating range of the specific engine, during the induction and, especially compression stroke.

Finally, similar velocity data are presented for all five cases studied at point C (Fig. 10), which is located at the center and close to the top of the main cylinder. This point is considered critical, as it is

close to the hypothetical position of the spark gap in an engine with more conventional design than the one investigated in the present study. Fig. 10 confirms that the compression ratio effect is quite strong during the induction stroke, while the engine speed does not differentiate the velocity patterns significantly.

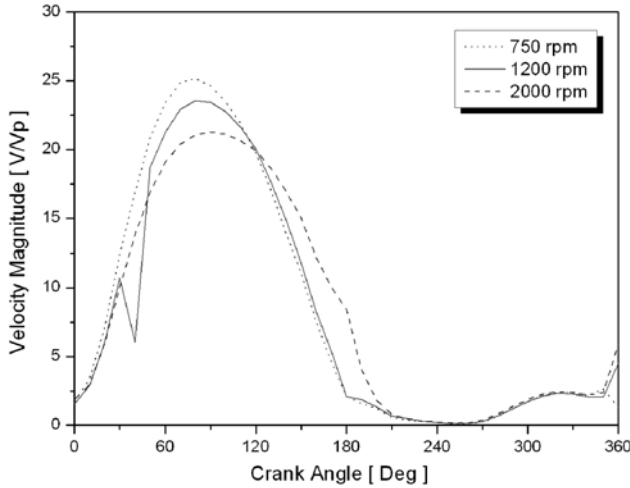


Fig. 9 Mean velocity variations at point B vs. CA at three eng. speeds, CR=5.7

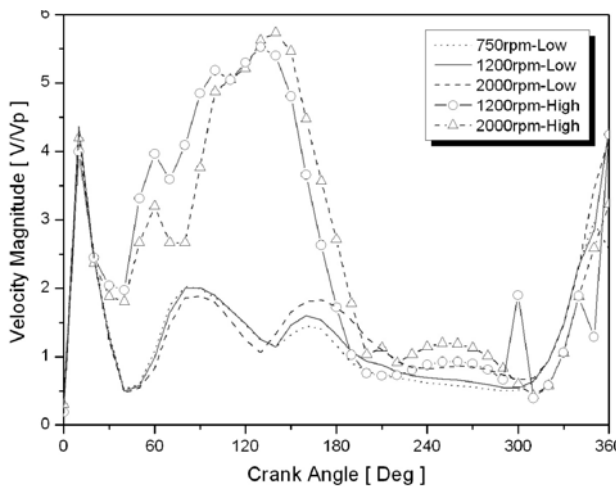


Fig. 10 Mean vel. variations at point C vs. CA at all five cases, low, CR=5.7, high CR=10

In order to have a better understanding of the in-cylinder flowfield, two-dimensional vector plots are presented for specific cross-sections at characteristic CA. The cross-sections selected are shown in Fig. 11: “I” is the plane which includes the two valve axes, II is the plane, parallel to the previous one, which divides the cylinder it two halves. The former was selected in order to visualize the flow entering through the valves, the latter to depict the main in-cylinder flow structures.

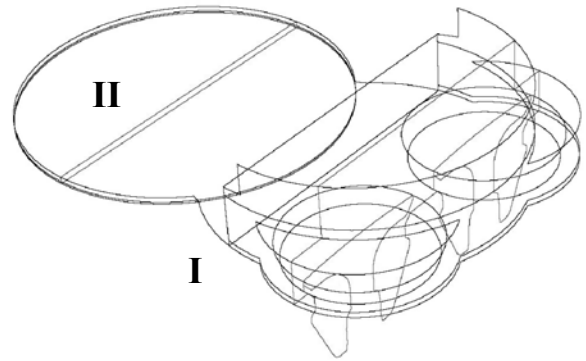


Fig. 11 Cross-sectional planes for the 2D vector plots

Fig. 12 presents two cases, corresponding to the two CRs, at cross section I at mid-induction stroke, i.e. 90° CA after TDC. At that CA the inlet valve is open almost at maximum valve lift and the piston is moving at maximum speed.

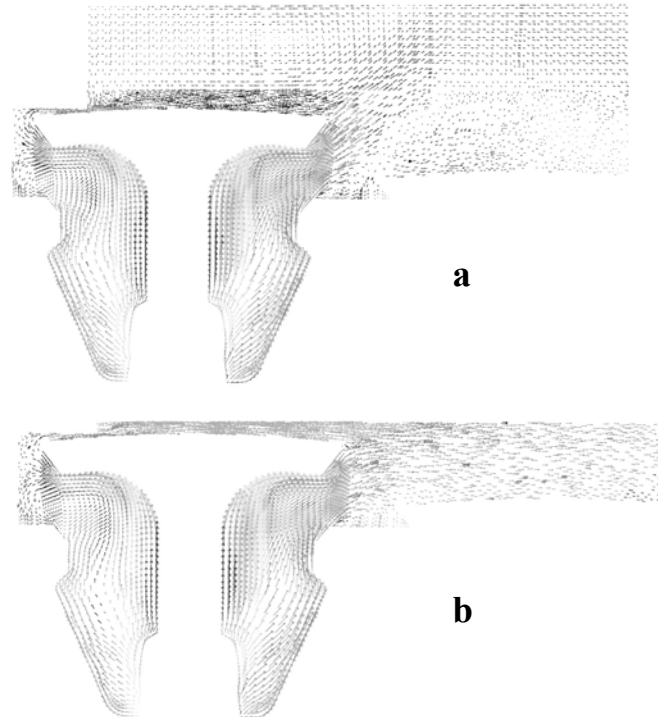
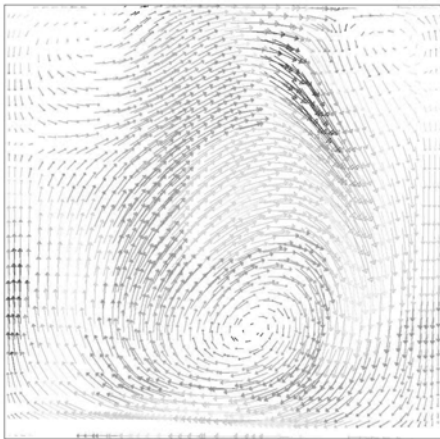


Fig. 12 Vector plots at section I at 90° CA after TDC of induction: a) 1200rpm & CR=5.7, b) 1200rpm and CR=10

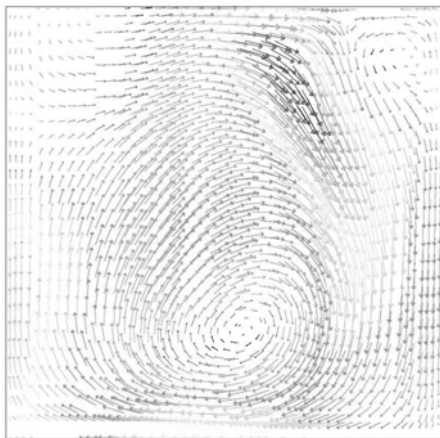
The mixture flow rate through the valve is quite high, with the maximum velocities appearing close to the valve stem inside the inlet port, as evidenced by both vector plots; this can be attributed to the orientation and the right angle (90°) shape of the inlet port (see Fig.1). However, the absolute values differentiate, depending on compression ratio, with the higher values associated, surprisingly, with the low compression ratio. The latter can be explained from the specific geometry employed in order to

modify the compression ratio: more specifically, the upper piston moving downwards to lower the combustion chamber volume, – and thus to increase the compression ratio – effectively diminishes the distance that the fluid travels when entering the cylinder, as can be seen in Fig. 12 b and Fig. 1.

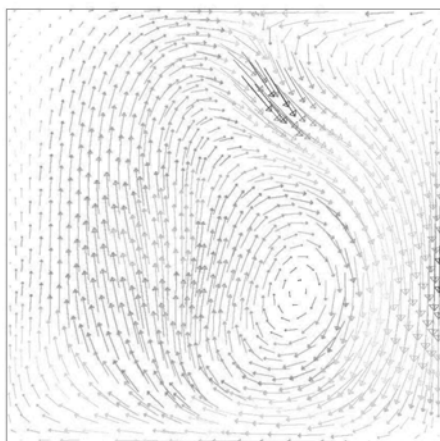
More insight on the in-cylinder flow structure can be revealed by the vector plots at section II at the end of the induction stroke or BDC (Fig. 13). All four flow-patterns are dominated by a major vortex, which is known as “tumble” or tumbling motion [3]. In most engines, this motion is created by the inlet port (or ports in the case of two or more inlet valves).



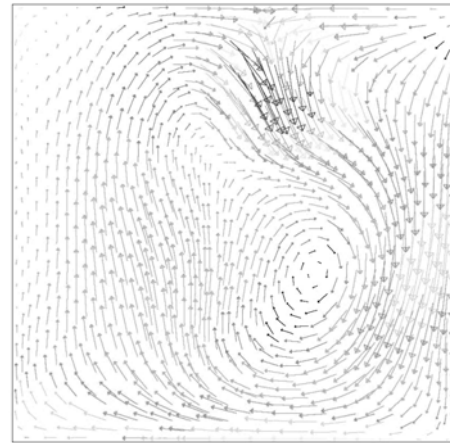
a



b



c



d

Fig. 13 Vector plots at section II at the BDC of induction: a, 1200rpm & CR=5.7, b, 2000rpm & CR=5.7, c, 1200rpm and CR=10, d, 2000rpm and CR=10

In the present engine configuration, the tumbling motion is mainly created by the geometry of the extended combustion chamber and the inlet valve position. Absolute velocity values depend both on speed and compression ratio, with the latter being the dominant factor. At the CR of 10 (Figs 13 c and d) maximum velocity values are much higher than in the case of CR of 5.7, confirming that the tumbling motion is stronger for the same engine speed. Finally, Figs. 13 a and b show that the weaker main vortex in the case of the lower compression ratio is associated with the existence of two smaller counter-rotating vortices at the two top corners close to the engine head.

## 6 Conclusion

A theoretical investigation involving a variable compression spark-ignition laboratory engine was performed. A commercial CFD package was employed to study the effect of engine speed and compression ratio on the in-cylinder flowfield during the whole operating cycle, with the emphasis being placed on the induction and compression stroke. Ensemble-averaged mean velocity data are presented in two main forms: normalised velocity magnitude at characteristic points as a function of crank angle and two-dimensional velocity vector plots at characteristic cross sections inside the cylinder and combustion chamber at specific crank angles. Results confirm that the in-cylinder flow scales well with engine speed, apart from early induction where there are noticeable differences. The compression ratio plays a more dominant role on the development of the in-cylinder flow, resulting in more pronounced bulk fluid movements. The

latter is particularly supported by the 2D vector plots, which reveal that, in the case of higher compression ratio, the mixture tumbling motion is stronger in quantitative terms at BDC, but also different in qualitative terms, with the disappearance of secondary vortices.

## 5 Acknowledgement

This research work was co-funded by the European Social Fund and National resources (EPEAEK II) Archimedes II.

### References:

- [1] Drake, M.C. and Haworth, D.C. "Advanced gasoline engine development using optical diagnostics and numerical modeling", *Proc. Combust. Inst.*, Vol. 31, 2007, pp. 99-124.
- [2] FLUENT 6.2. User's Guide, Fluent Inc., 2005.
- [3] Jafri, K., Hasher HG, Novak M., Lee K., Schock H., Bonne M, "Tumble and swirl quantification within a motored four-valve SI engine cylinder based 3-D LDV measurements", SAE paper No 970792, 1997.
- [4] Kamura, H. and Takada K, "Development of in-cylinder gasoline direct injection engine", *JSAE Review*, Vol. 19, 1998, pp.175-180
- [5] Patankar, VS, *Numerical Heat Transfer and Fluid Flow*, Washington, Hemisphere Publishing Corp. , 1980.
- [6] Stobart, R.K., *Fuel cell Technology for Vehicles 2002-2004*, SAE International, 2004.
- [7] Zimont, V.L. and Lipatnikov, A.L., "A numerical Model of Premixed Turbulent Combustion of Gases", *Chem. Phy. Report*, 14(7), 1995, pp. 993-1025.
- [8] Zimont, V.L., Polifke, W., Bettelini, M. and Weisenstein, W. "An efficient Computational Model for Premixed Combustion at High Reynolds Numbers Based on a Turbulent Flame Speed Closure", *J. of Gas Turbines Power*, Vol. 120, 1998, pp. 526-532.
- [9] Zimont, V.L., "Gas Premixed Combustion at High Turbulence. Turbulent Flame Closure Model Combustion Model", *Experimental Thermal and Fluid Science*, Vol. 21, 2000, pp. 179-186